FISEVIER

Contents lists available at ScienceDirect

### Materials Science & Engineering A

journal homepage: http://www.elsevier.com/locate/msea





# Competitive relationship during fatigue-crack initiation of friction-stir-welded Al alloy

Zepeng Liu<sup>a</sup>, Hongxia Zhang<sup>a</sup>, Zhenguo Hou<sup>b</sup>, Zhifeng Yan<sup>a</sup>, Peter K. Liaw<sup>c</sup>, Peng Dong<sup>a,\*</sup>

- a College of Materials Science and Engineering, Taiyuan University of Technology, Taiyuan, 030024, China
- <sup>b</sup> Department of Special Welding Processes, CRRC Tangshan Co, Ltd, Tangshan, 063035, China
- <sup>c</sup> Department of Materials Science and Engineering, The University of Tennessee, Knoxville, TN, 37996, USA

#### ARTICLE INFO

# Keywords: Aluminum alloy Surface treatment Stress intensity factor range FGA Fatigue life prediction

#### ABSTRACT

In the present work, uniaxial fatigue tests (R=0.1) showed that for high-strength aluminum alloys, the crack origin also presented a tendency of transition from the outside to the inside with the stress decreasing. The interior crack-initiation mode has a characteristic of a fish-eye embracing fine granular area (FGA) originated from an inclusion. Moreover, the formation mechanism of FGA was discussed. The values of the stress intensity factor (SIF) range of a surface mode and an internal mode were calculated. The results showed that  $\Delta K_{FGA}$  keeps constant with an average value of  $1.84~\mathrm{MPa} \bullet \mathrm{m}^{1/2}$ , which was close to the interior crack-growth threshold ( $\Delta K_{\mathrm{th}}$ , j),  $1.911~\mathrm{MPa} \bullet \mathrm{m}^{1/2}$ . Paris-Hertzberg law was used to predict the life of fatigue-crack initiation and propagation during internal fracture. The crack-growth rate within FGA and fish-eye was also estimated. Furthermore, the competitive relationship between the interior and surface cracks initiation of welded joints was discussed through the SIF range.

#### 1. Introduction

In the 1980s, Naito et al. [1,2] found that the fatigue fracture of carburizing steels can occur at  $10^7$  cycles or even more than  $10^8$  cycles. In the later decades, such failure phenomena were also found in high-strength steels [3–9], and was defined as the very high cycle fatigue (VHCF). Since the first international conference on VHCF initiated by Professor Bathias [10] in Paris, France in 1998, research on VHCF has received extensive attention, making the traditional fatigue limit with-stand enormous challenges [11,12]. Most of research on VHCF of ferrous materials showed that the fatigue-crack-initiation site would change from the specimen surface to the interior of the specimen, forming the so-called internal fish-eye fracture surface. Besides, non-metallic inclusions were usually observed at the center of the fish eye, and were believed that they are responsible for the internal-crack initiation [7–9].

For the non-ferrous alloys, current works indicate that they will also fracture in the fatigue life above  $10^7$  cycles. Wang et al. [13] found that the fatigue failure can occur beyond  $10^7$  cycles and even at  $10^9$  cycles and beyond. No endurance limit could be found in the 7075-T6 and 6061-T6 aluminum alloys until  $10^9$  cycles. However, the cycles corresponding to the failure-mode transition (the specimen surface to the interior of the specimen) of these alloys are different from those of steels.

For instance, Al and Mg alloys occur usually above  $10^8$  cycles [14,15], whereas  $10^6$ – $10^7$  cycles for most steels. Clearly, fatigue life is not suitable for judging whether interior fatigue failure occurs.

For fatigue failure, it is generally accepted that there is a competitive relationship between surface and internal modes. In case of metallic materials with internal defects (inclusions or pores), internal-crack initiation is dominant at low stress amplitudes and high numbers of cycles, whereas surface-fatigue crack initiation occurs at high stress amplitudes and low cycles. Therefore, there is a definite stress range where the crack-initiation site changes from the specimen surface to the interior of the specimen. In a specific environment, the stress range corresponding to the failure-mode transition of the metallic materials is the unique attribute of the material. When the size and position of internal defects change, the stress range will accordingly. Lei et al. [16] found that as the size of the inclusion increases, the stress amplitude corresponding to the failure mode transition decreases. Furthermore, changes in the external environment, including temperature [17], loading mode (stress ratio [18] and loading frequency [19]) and corrosive environments [20], etc., will also affect the stress range corresponding to internal and external crack-initiation competition. When the material is subjected to surface treatment, the surface state of the material changes, which inhibits the initiation of fatigue cracks from the

\* Corresponding author.

E-mail address: dongpeng@tyut.edu.cn (P. Dong).

surface and intervenes in the transition vary of failure modes. Shiozawa et al. [21] found that the compressive residual stress introduced by shot peening would change the stress level and cycles corresponding to the transition of failure modes. Our previous research [22] on the friction-stir-welded 7075-T651 aluminum alloy showed that the fatigue-crack initiation of the as-welded joint when the fatigue life reaches  $10^7$  cycles is still the surface mode. However, due to the effect of SMRT, the failure-mode transition occurred in advance (at  $\sim 10^6$  cycles). This feature means that the intervention of SMRT makes fatigue-crack initiation from the surface of the specimen to interior under high stress and low cycle conditions.

On fracture surfaces resulting from interior-crack initiation and propagation in a VHCF regime, a distinctive feature is observed in the vicinity of a non-metallic inclusion at the fracture origin inside the fisheye zone. This area was named as a fine granular area (FGA) by Sakai et al. [23,24], granular-bright facet (GBF) by Shiozawa et al. [25,26], and optically-dark area (ODA) by Murakami [27]. They have the same morphology but are named differently because the contrasts observed on different instrumentations are different. Hong et al. [28] found that a nanograin layer of a fine granular area (FGA) region prevails for the cases of negative stress ratios in the interior failure of high-strength steels, and attributed the formation of FGA to Numerous Cyclic Pressing (NCP), which is different from other FGA formation mechanisms, such as hydrogen embrittlement-assisted cracking by Murakami [29], dispersive decohesion of spherical carbides by Shiozawa et al. [25,30], and polygonization and debonding by Sakai [31,32]. Furthermore, Sakai et al. [23] pointed out that the value of the stress intensity factor range for FGA  $\Delta K_{\text{FGA}}$  was close to the threshold value for stable crack propagation in SUJ2 steel,  $\Delta K_{\text{th}}$ . This quantitative parameter of FGA provides a theoretical foundation for studying the life of crack-initiation in VHCF and the crack-extension rate within FGA [33.34].

It is practical and important to know that how and when a failure mode changes in the long fatigue life range, especially for heterogeneous materials, such as welded joints. In the present work, the stress intensity factor range ( $\Delta K$ ) is used to reveal the competitive relationship in the failure mode transition process.

#### 2. Experimental details

A commercial 7075-T651 aluminum alloy (produced by Alcoa Inc.) is used as the base metal (BM) in the present study, with a nominal thickness of 25 mm. The chemical composition of the 7075-T651 aluminum alloy is (in weight percent): 5.70 Zn, 2.53 Mg, 1.66 Cu, 0.26 Fe, 0.22 Si, 0.20 Cr, 0.18 Mn, 0.08 Ti, and the rest amount for Al.

Double-sided FSW (CFSW; LM-AM16-2D) was performed on plates with the size of 500 mm (length)  $\times$  150 mm (width)  $\times$  25 mm (thickness). The selected welding parameters and the welding tool are shown in Fig. 1. After welding, dog-bone-shaped samples used for fatigue tests were prepared, some of which were subjected to surface mechanical rolling treatment (SMRT). Because welded joints without SMRT would

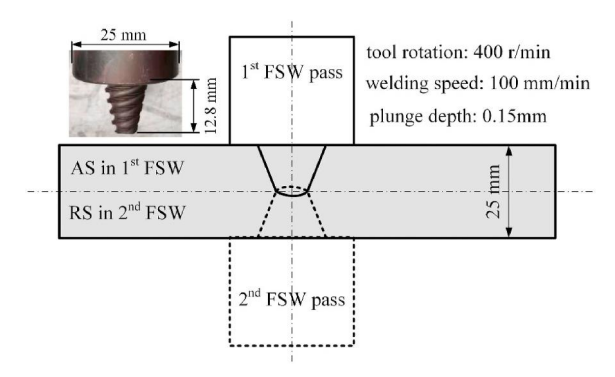


Fig. 1. Schematics of double-sided FSW.

not present internal fractures even if it exceeds  $10^7$  cycles, SMRT was used to make internal fractures occur under high stress and low cycles. Detailed descriptions of SMRT procedures and the microstructure characterization of the gradient grain layer generated after the SMRT might be referred to our previous work [22].

Fatigue tests were conducted on an electro-magnetic fatigue testing machine (CRIMS GPS200) at room temperature under the stress-control mode with a stress ratio of 0.1 and a frequency of  $\sim$ 100 Hz.

Fractography analysis of the fatigue-fracture samples was carried out employing scanning electron microscopy (SEM; TESCAN MIRA3 LM). Transmission electron microscopy (TEM; FEI Tecnai G2 F20 S-Twin) was used to research the matrix/particle boundary and performed with an acceleration voltage of 200 kV. The TEM foil was prepared, using the focused ion beam (FIB; FEI Helios Nanolab 600i DualBeam System) and lift-out techniques.

#### 3. Results

Fig. 2 shows fatigue-testing results of FSWed joints. Clearly, the crack-initiation position of the as-welded joint is always the surface mode, even if the fatigue life exceeds  $10^7$  cycles. However, the fatigue-crack initiation has a surface mode and interior mode for the SMRTed joints. When the  $\sigma_{\rm max} < 307$  MPa, fatigue-crack initiation is located in the interior of the SMRTed joints.

Fig. 3 shows two sets of SEM images of the surface-initiation model of the FSW joint, with and without SMRT. The fracture morphologies for a SMRTed joint and welded joint failed at  $N_{\rm f}=1.02\times10^5$  and  $N_{\rm f}=7.83\times10^4$ , respectively, with the maximum stress ( $\sigma_{\rm max}$ ) of 350 MPa, are plotted in Fig. 3a and b, respectively. For metallic materials subjected to cyclic loadings, it is not surprising that the surface inclusion acts as the initiation site of the fatigue crack.

As the stress level decreases below the critical value, it is clearly seen that the fatigue-crack initiation is located in the interior of the welded joints after SMRT. The SEM results shown in Fig. 4 are examples of a typical morphology of interior-crack initiation for the SMRTed joints failed at  $N_{\rm f}=4.98\times10^6$  with the maximum stress ( $\sigma_{\rm max}$ ) of 303 MPa (Fig. 4a–c) and  $N_{\rm f}=6.63\times10^6$  with the maximum stress ( $\sigma_{\rm max}$ ) of 300 MPa (Fig. 4d–f). Multiple fracture morphologies indicate that the internal fracture characteristics of aluminum alloys are similar to those of "fish-eye" fractures in high-strength steels suffered VHCF [28], as shown in Fig. 4a and d. The dark area within the yellow dotted line (Fig. 4a and d) is a typical area of the "fish-eye" (FiE) morphology, and the center of which is the metal inclusion that induces the initiation of interior cracks. The TEM results [22] showed that the inclusion is an  $Al_{18}Ti_2Mg_3$  constituent phase (Fig. 4b and e). It is seen from Fig. 4c and f, the area of the

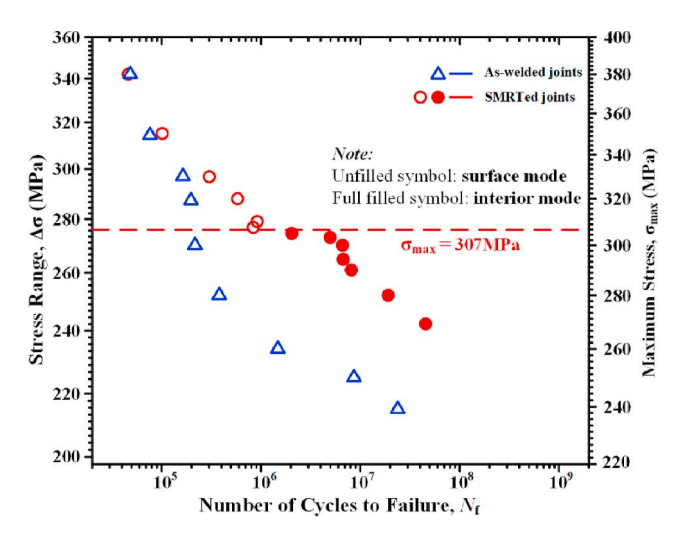


Fig. 2. S-N curves of as-welded and SMRTed joints.

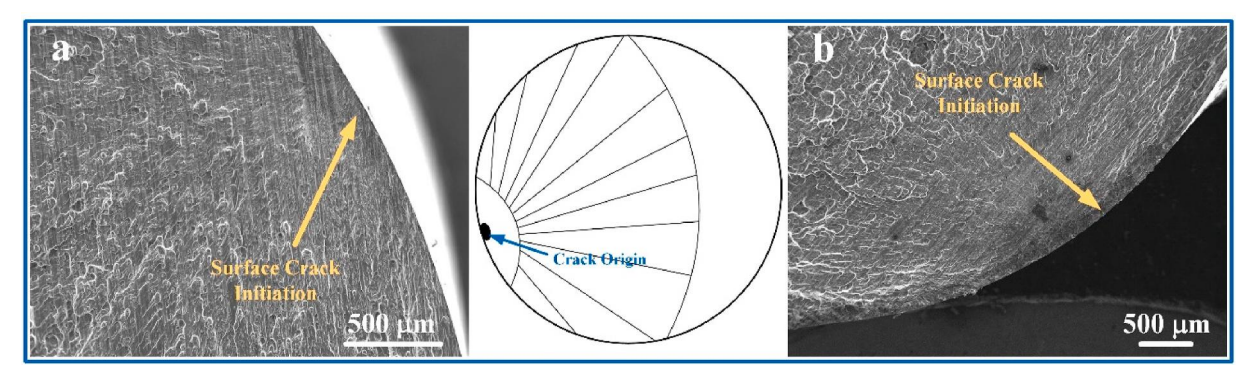


Fig. 3. SEM images of the fracture surface of the SMRTed joint (a) and as-welded joint (b) under  $\sigma_{max}$  of 350 MPa, both showing the surface-initiation mode.

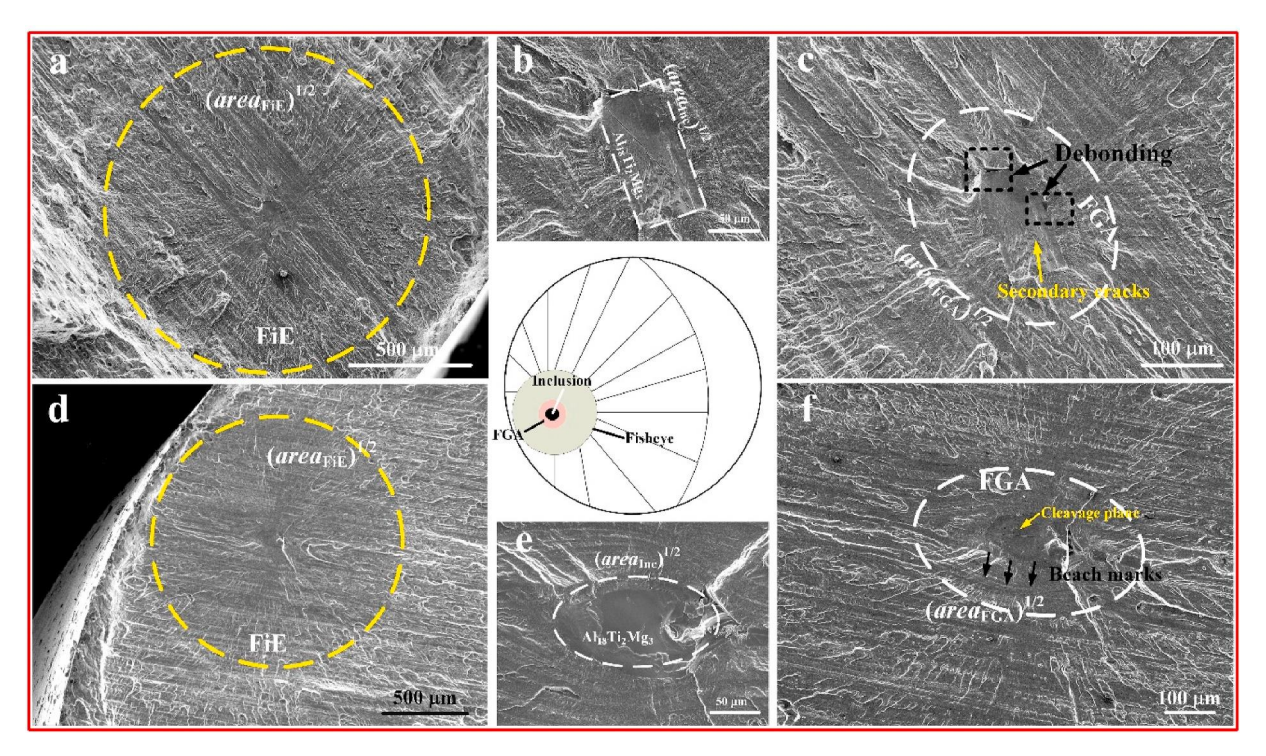


Fig. 4. SEM images of the fracture surface of SMRTed joints with interior-initiation cracking under the maximum stress of 303 MPa,  $N_f = 4.98 \times 10^6$  (a–c), and 300 MPa,  $N_f = 6.63 \times 10^6$  (d–f).

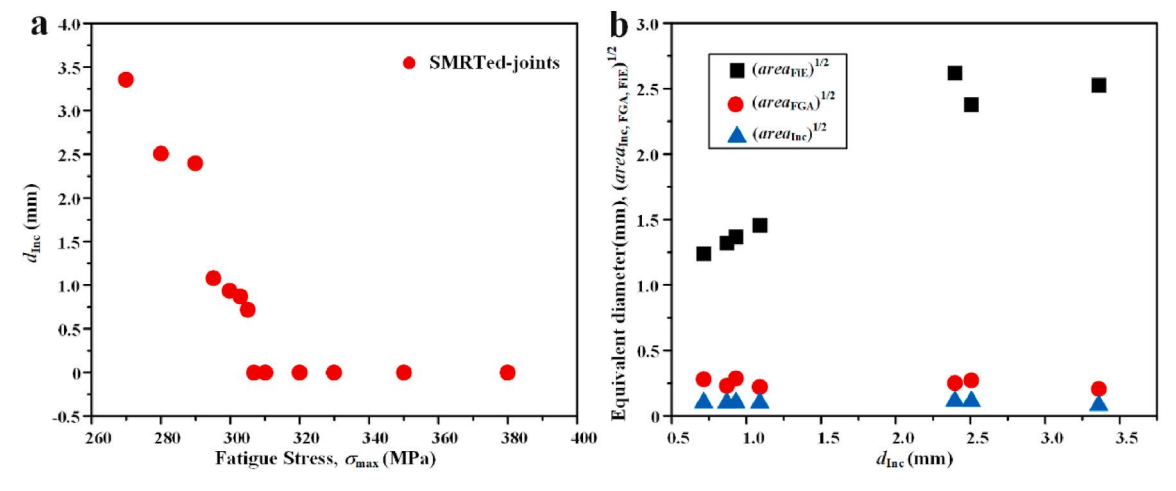


Fig. 5. Depth of the inclusions from the surface,  $d_{\rm Inc}$  as functions of the fatigue stress,  $\sigma_{\rm max}$  (a), equivalent diameter,  $(area_{\rm Inc,\ FGA,\ FiE})^{1/2}$ , as a functions of  $d_{\rm Inc}$ .

white dashed line outside the inclusion is the FGA. Also, from Fig. 4f, the transition area from elliptical extension traces ("beach marks") to rolled grain boundaries is clearly visible, and it is considered that the periphery of FGA has been reached.

It can be found that the outline of the FiE is a very standard circle, regardless of the shape of the irregular inclusions. As shown in Fig. 4a, the region of the FiE (dark area, equivalent diameter of 1.32 mm) is related to the depth of the inclusions from the surface. To obtain these equivalent diameters,  $(area_{Inc})^{1/2}$ ,  $(area_{FGA})^{1/2}$ , and  $(area_{FiE})^{1/2}$  are used, with the values of areas being measured from SEM images. On the other hand, the size of the surface-crack initiation site,  $(area_{Inc})^{1/2}$ , which is defined as the size of the facet formed by the crystalline slip, that is, the Stage-I crack-growth zone depends on the stress amplitude [25]. As the stress amplitude decreases for SMRTed joints, the distance from the crack-initiation position ( $d_{Inc}$ ) to the surface layer increases, as shown in Fig. 5a. In addition, the  $(area_{FiE})^{1/2}$  is proportional to  $d_{Inc}$ , which means that the maximum distance that the periphery of the FiE can reach is the surface layer (Fig. 5b). However, the size of  $(area_{FGA})^{1/2}$ and  $(area_{Inc})^{1/2}$  remains stable, and does not change with changes in stress and distance from the surface.

#### 4. Discussion

#### 4.1. Crack-initiation and FGA formation

In order to study the internal crack-initiation and early growth process of the Al alloy, the TEM foil, containing both particle and an adjacent matrix, is prepared using a FIB system (inserted in Fig. 6a). For this research, HRTEM results show that there is an obvious difference in the orientation of the atomic arrangement between the  $\alpha$ -Al matrix and the particle (Al $_{18}$ Ti $_{2}$ Mg $_{3}$ , the atomic orientation shown by the yellow arrow in Fig. 6a), forming a structure disorder zone at the interface (Fig. 6a), the corresponding atomic schematic diagram of the matrix/particle boundary shown in Fig. 6b. After cyclic loading being loaded, the structural disorder zone acts as a trap. As a result, the dislocation density within the disorder zone increases with cycles, resulting in the partial debonding of the matrix/particle interface, as shown in the black dotted rectangle in Fig. 4c.

Fig. 7 is a schematic drawing of interior-crack initiation and FGA formation. The interface debonding occurs, could be regarded as the initial crack, and first propagates within the particle, followed by a cleavage fracture of the  $\mathrm{Al}_{18}\mathrm{Ti}_2\mathrm{Mg}_3$  constituent phase, as shown in Fig. 7. The existence of cleavage planes can be found on the particle fracture morphologies shown in Fig. 4c and f. Then, the crack-extension is hindered by the rolled grain. The coarse grains within the matrix adjacent to the particle are broken down to fine grains at the crack tip by repeated pressing between the crack surfaces. In the subsequent crack-propagation process, the crack-extension rate is extremely slow,

leaving an elliptical extension trace on the fracture surface ("beach marks", as presented in Fig. 4f) due to the inside of the material is in a vacuum environment. Schönbauer [35] found that fatigue-crack propagation in vacuum still takes place at a rate of  $5\times 10^{-13}$  m/cycle, which is several decades below the theoretical value of one lattice space per cycle. When the "beach marks" gradually disappear, and the rolled grain boundaries are clearly visible, it is considered that the periphery of FGA has been reached.

Generally, physically-short cracks have a crack length smaller than ten times the average grain size (a < 10d) [9]. The distance from the interface of the particle/Al matrix to the periphery of the FGA is about 44  $\mu m$ , which is less than 10 times the grain width (50  $\mu m$ ), accorded with the characteristics of short crack propagation in FGA. The formation mechanism of FGA in the Al alloy is obvious different from FGA in high-strength steels. In addition, grain refinement is observed in the Al alloy but no a layer of nanograins is found. In order to distinguish this area from the FiE, the characteristic area in the aluminum alloy is also called FGA by borrowing the definition of fine granular area (FGA) by Sakai et al. [23]. But for the other materials, 40Cr studied by Oian et al. [36] had shown that although there was no clear trace of FGA surrounding inclusions, there was still a region whose roughness (37.9 nm) was larger than that of fish-eve region (11.3 nm). That is to say, the existence of nanograin layer is not the only criterion for judging the FGA.

#### 4.2. Stress intensity factor range

The values of stress intensity factor ranges of a surface mode and interior mode are calculated, using the following Eq. (1) [37]:

$$\Delta K_{\text{Inc,FGA or FiE}} = A\sigma_{\text{a}}\sqrt{\pi\sqrt{area_{\text{Inc,FGA or FiE}}}}$$
 (1)

where A is 0.5 for an interior fracture and 0.65 for a surface fracture,  $\sigma_a$  is the amplitude of the fatigue stress in MPa. For interior mode, the square root (SQRT) of the area is an equivalent size of an inclusion (Al<sub>18</sub>Ti<sub>2</sub>Mg<sub>3</sub> constituent phase), FGA or fish-eye where SQRT of the area is in m, and  $\Delta K$  is in MPa•m<sup>1/2</sup>. The  $area_{Inc}$  when the cracks initiate on the surface is the projected area where the small cracks reach stable extension [38].

Fig. 8 shows the relationship between the SIF range,  $\Delta K_{\rm Inc, FGA \ or \ FiE}$  and fatigue stress,  $\sigma_{\rm max}$ . For the surface mode, the SIF ranges of aswelded and SMRTed joints have a tendency to decline as the stress decreases.  $\Delta K_{\rm Inc}$  in the range of the maximum stress ranging from 380 MPa to 250 MPa is 3.62-2.37 MPa $\bullet$ m<sup>1/2</sup> for as-welded joints. As a comparison,  $\Delta K_{\rm Inc}$  of SMRTed joints in the range of the maximum stress ranging from 380 MPa to 307 MPa is 2.48-1.92 MPa $\bullet$ m<sup>1/2</sup>. It can be found that SMRT significantly reduces the SIF range when cracks initiate from the surface. Then the threshold SIF for the surface-crack-growth,  $\Delta K_{\rm th,s}$ , is

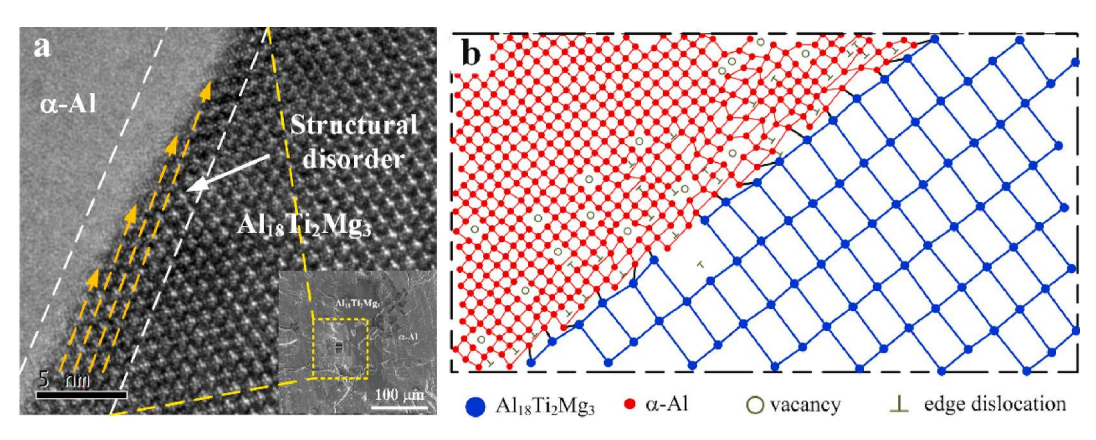


Fig. 6. Original HRTEM image taken from the matrix/particle boundary (a), showing a structural disorder zone, and corresponding atomic schematic diagram (b).

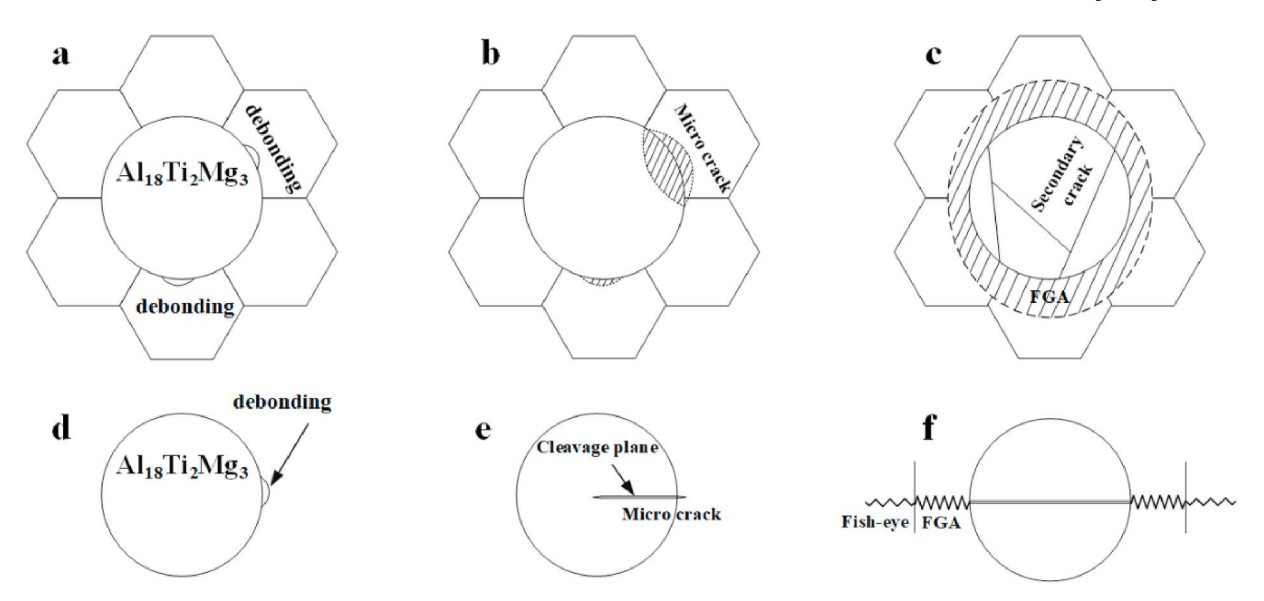
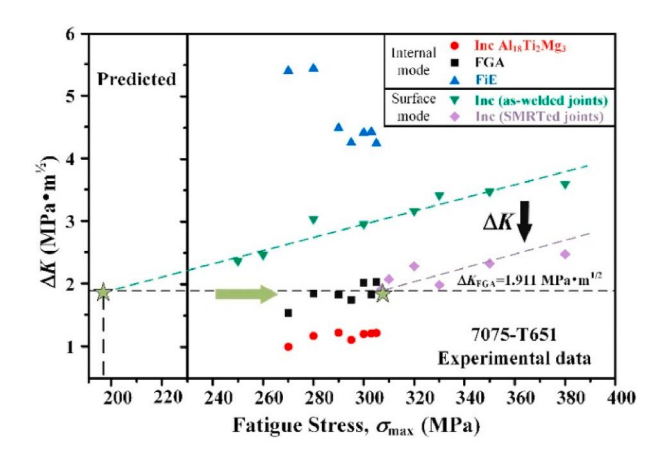


Fig. 7. Schematic drawing of interior-crack initiation and FGA formation, top view of a fracture plane (a–c), front view of a fracture plane (d–f), partial debonding of the matrix/particle interface (a, d), micro-crack initiation and particle cleavage fracture (b, e), secondary cracks occurring in a particle and formation of FGA (c, f).



**Fig. 8.** Stress intensity factor range as a function of the fatigue stress for SMRTed and welded joints.

estimated to be 1.92 MPa $\bullet$ m<sup>1/2</sup>. Therefore, a surface crack cannot occur and propagate at a surface defect below the  $\Delta K_{\text{th,s}}$ .

For the interior fracture,  $\Delta K_{\rm FiE}$  is in the range of 4.26–5.92 MPa $\bullet$ m<sup>1/2</sup>, with an increasing trend as the stress decreases. For Inc and FiE,  $\Delta K_{\rm Inc}$  and  $\Delta K_{\rm FGA}$  are in the range of 1.02–1.23 MPa $\bullet$ m<sup>1/2</sup> and 1.54–2.04 MPa $\bullet$ m<sup>1/2</sup>, respectively, with averages of 1.17 and 1.84 MPa $\bullet$ m<sup>1/2</sup>, respectively, indicating that the SIF range of FGA and Inc is almost a constant. The FGA theoretical SIF range calculation formula [34] is:

$$\Delta K_{\text{FGA}} = \mu \sqrt{6\pi b} = 4.342\mu \sqrt{b} \tag{2}$$

where  $\mu$  is shear modulus, and b is Burgers vector. For Al alloys,  $b\approx 0.2863$  nm,  $\mu\approx 26$  GPa, the predicted thresholds are 1.911 MPa $\bullet$ m<sup>1/2</sup>, which can be recognized as the threshold SIF range for interior stable micro-crack propagation ( $\Delta K_{\text{th,i}}$ ) [34]. It is proposed that for crack interior initiation mode, there exists an intrinsic characteristic size related to  $\Delta K_{\text{th,i}}$ . The calculated  $\Delta K_{\text{FGA}} = 1.84$  MPa $\bullet$ m<sup>1/2</sup> is close to the  $\Delta K_{\text{th,i}}$ . Therefore,  $\Delta K_{\text{FGA}}$  can be used to predict the threshold of stable fatigue-crack growth. It is expected that the internal crack generated at an inclusion will propagate after formation of the FGA in the vicinity of the inclusion for long-life fatigue. Clear similar values between  $\Delta K_{\text{th,i}}$  and  $\Delta K_{\text{th,i}}$  were obtained from this tested material, which is about 1.911 MPa $\bullet$ m<sup>1/2</sup>.

#### 4.3. Fatigue life prediction

Since the value of  $\Delta K_{\text{FGA}}$  corresponds to that of  $\Delta K_{\text{th,i}}$ , the fatigue life for the formation of the FGA is considered to be the crack-initiation life. For internal fracture, fatigue life consists of three parts: (1) micro-crack initiation ( $N_{\text{FGA}}$ ), (2) stable micro-crack propagation ( $N_{\text{FGA}}$ ), and (3) unstable macro-crack propagation and fracture ( $N_{\text{FGA}}$ ). Since the life consumed by unstable macro-crack propagation is extremely short, it can be ignored, making  $N_{\text{f}} = N_{\text{FGA}} + N_{\text{FGA}}$ . Paris et al. [38] have shown a historical review on crack-growth and threshold to develop the estimation procedure for crack-growth life for internal initiation and predicted the threshold corner at:

$$\frac{\mathrm{d}a}{\mathrm{d}N} = b \text{ and } \frac{\Delta K_{\mathrm{eff}}}{E\sqrt{b}} = 1$$
 (3)

where b is the Burger's vector, E is Young's modulus and  $\Delta K_{\rm eff}$  is the effective stress intensity factor. The corresponding crack-growth Paris-Hertzberg law is used to estimate the life of the small cracks in the fisheye range, considering the crack closure is minimal for this type of crack:

$$\frac{\mathrm{d}a}{\mathrm{d}N} = b \left(\frac{\Delta K_{\mathrm{eff}}}{E\sqrt{b}}\right)^{3} \tag{4}$$

The stress intensity factor,  $\Delta K$ , can be calculated via:

$$\Delta K = \frac{2}{\pi} \Delta \sigma \sqrt{\pi a} \tag{5}$$

The crack size, a, in Eq. (5) is calculated as the SQRT of the crack area. The integration of the Paris-Hertzberg law to determine the crack-growth life, will begin here with the crack-growth rate corner, which one will denote as  $\Delta K_{\text{FGA}}$  corresponding to an initial SQRT of the crack area,  $a_{\text{FGA}}$ . Substituting these into Eq. (4)

$$\frac{\mathrm{d}a}{\mathrm{d}N} = b \left(\frac{\Delta K_{\mathrm{FGA}}}{E\sqrt{b}}\right)^{3} \left(\frac{a}{a_{\mathrm{FGA}}}\right)^{3/2} = b \left(\frac{a}{a_{\mathrm{FGA}}}\right)^{3/2} \tag{6}$$

Thus, Eq. (3) can be rewritten as:

$$1 = \frac{\Delta K_{\text{FGA}}}{E\sqrt{b}} = \frac{2\Delta\sigma\sqrt{a_{\text{FGA}}}}{\sqrt{\pi}E\sqrt{b}} \text{ or } a_{\text{FGA}} = \frac{\pi E^2 b}{4(\Delta\sigma)^2}$$
 (7)

Eq. (6) can be integrated from  $a_{FGA}$  to  $a_{FiE}$ , which gives:

$$N_{\text{FGA}\to \text{FiE}} = \frac{(a_{\text{FGA}})^{3/2}}{b} \int_{a_{\text{FG}}}^{a_{\text{FiE}}} \frac{da}{a^{3/2}} = \frac{\pi E^2}{2(\Delta \sigma)^2} \left[ 1 - \sqrt{\frac{a_{\text{FGA}}}{a_{\text{FiE}}}} \right]$$
(8)

The fatigue life for the stable micro-crack propagation stage in Eq. (8) can be rewritten as:

$$N_{\text{FGA}\to\text{FiE}} = \frac{\pi E^2}{2\sigma_a^2} \left[ 1 - \sqrt{\frac{a_{\text{FGA}}}{a_{\text{FiE}}}} \right] \tag{9}$$

The fatigue life for the formation of the FGA can be predicted as  $N_{\rm FGA} = N_{\rm f} - N_{\rm FGA \to FiE}$ . The results of  $N_{\rm FGA}$  and  $N_{\rm FGA \to FiE}$  for each specimen are listed in Table 1. Correspondingly, the values of  $N_{\rm FGA}/N_{\rm f}$  and  $N_{\rm FGA \to FiE}/N_{\rm f}$  for each specimen are obtained (listed in Table 1 and plotted in Fig. 9). Apparently, the fatigue life consumed by the stable micro-crack propagation stage is very short, in the range of  $2.2 \times 10^5 - 3.8 \times 10^5$  cycles. For comparison, the ratio of  $N_{\rm FGA}/N_{\rm f}$  increases with the decrease of stress, and for the total fatigue life beyond  $10^7$  cycles, the value of  $N_{\rm FGA}/N_{\rm f}$  is larger than 98%, or over than 99% of  $N_{\rm f}$ .

The values of average crack-growth rate within FGA were calculated from the FGA size and the fatigue life consumed by this region following Eq. (10), and the results are shown Table 2. The results show that as the fatigue life increases, the crack-growth rate in the FGA decreases. For  $N_{\rm f}$  between  $10^6$  and  $10^7$ , the values of  $({\rm d}a/{\rm d}N)_{\rm FGA}$  are within the range of  $10^{-11}$ – $10^{-12}$  m/cycle. When the fatigue life is higher than  $10^7$  cycles, the order of magnitude of  $({\rm d}a/{\rm d}N)_{\rm FGA}$  enters the order of  $10^{-12}$  m/cycle. For the stable crack-growth stage outside the FGA, Eq. (11) is used to calculate the crack-growth rate  $({\rm d}a/{\rm d}N)_{\rm FiE}$ . For internal fractures, the order of magnitude of the crack-growth rate is about  $10^{-9}$  m/cycle.

$$\overline{\left(\frac{\mathrm{d}a}{\mathrm{d}N}\right)}_{\mathrm{FGA}} = \frac{\sqrt{area_{\mathrm{FGA}}} - \sqrt{area_{\mathrm{Inc}}}}{N_{\mathrm{f}} - N_{\mathrm{FGA} \to \mathrm{FiE}}} \tag{10}$$

$$\overline{\left(\frac{\mathrm{d}a}{\mathrm{d}N}\right)}_{\mathrm{FiE}} = \frac{\sqrt{area_{\mathrm{FiE}}} - \sqrt{area_{\mathrm{FGA}}}}{N_{\mathrm{FGA}\to\mathrm{FiE}}} \tag{11}$$

When the crack initiates inside, the relationship between the crackgrowth rate (da/dN) and the stress intensity factor  $(\Delta K)$  of the aluminum alloy as shown in Fig. 10 is fitted by combining different stresses. Fig. 10 reflects the two stages of crack-initiation and propagation. The crack-initiation rate is much higher than the propagation rate. Therefore, the threshold of fatigue-crack propagation for internal fractures  $(\Delta K_{\text{th},i})$  also can be obtained from the figure is about 2 MPa $\bullet$ m $^{1/2}$ .

## 4.4. Competitive relationship between the interior and surface crack initiation

When the fatigue-crack initiation of FSWed joints with and without SMRT in a surface-mode, there is no significant difference in the fatigue lifetimes between as-welded joints and SMRTed joints when the  $\sigma_{\rm max}>$  307 MPa. However, the initial SIF range of a surface defect of SMRTed joints is significantly lower than that of as-welded joints. Through the SMRT, a gradient grain layer is formed on the surface layer, compressive residual stresses, and gradient hardness layers are introduced, which effectively reduces the initial SIF range of the surface. Meanwhile, the strengthened surface layer attempts to prevent fatigue cracks from initiating from the surface. Nevertheless, since the initial SIF range of a

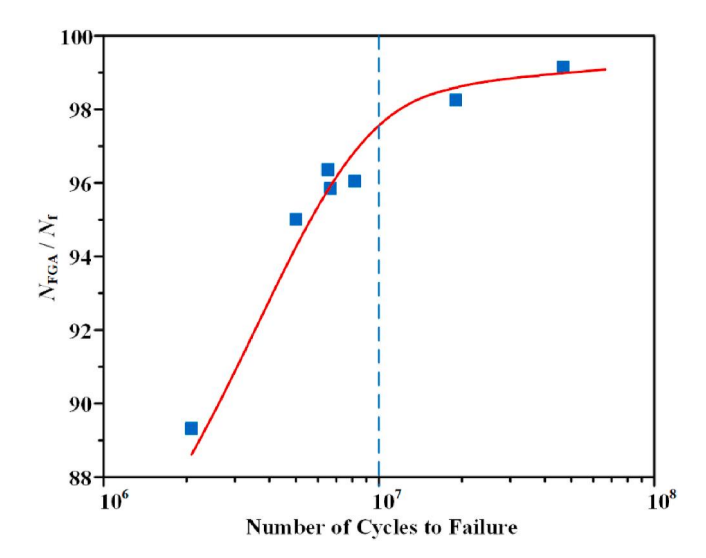


**Fig. 9.** Crack-initiation life, i.e. the fraction of fatigue life for the formation of the FGA, as a function of total fatigue life.

**Table 2** Crack-growth rate in FGA and FiE.

	-				
Specimen code	Fatigue stress, $\sigma_{\rm max}$ (MPa)	(da/dN) <sub>FGA</sub> (m/ cycle)	$(da/dN)_{FGA\rightarrow FiE}$ (m/cycle)		
1	305	$9.76 \times 10^{-11}$	$4.35 \times 10^{-9}$		
2	303	$2.78\times10^{-11}$	$4.39 \times 10^{-9}$		
3	300	$2.96  imes 10^{-11}$	$4.58  imes 10^{-9}$		
4	295	$1.92\times10^{-11}$	$4.51 \times 10^{-9}$		
5	290	$1.77\times10^{-11}$	$7.44 \times 10^{-9}$		
6	280	$8.59\times10^{-12}$	$6.38\times10^{-9}$		
7	270	$2.67 \times 10^{-12}$	$6.05\times10^{-9}$		

surface defect is greater than  $\Delta K_{\text{th,i}}$ , the fatigue cracks preferentially initiate from the surface when the stress is greater than 307 MPa.

Due to the reduction of the initial SIF range of a surface defect of SMRTed joints, it is noticed that the internal and external competition has already appeared when the  $\sigma_{\rm max}=307$  MPa. Below this value, a surface crack cannot occur and propagate, the internal SIF range has the upper hand, making cracks preferentially initiate from the interior. After that, the fatigue life is significantly improved, and the effect of SMRT is fully revealed. During the experiment, no internal fracture was found in the FSWed joints without SMRT, even if the fatigue life exceeds  $10^7$  cycles, which does not mean that there are no inclusions inside, but within the stress range of the whole experiment, the initial SIF range on the surface defect is much larger than  $\Delta K_{\rm th,i}$ .

According to the change trend of the SIF range of the as-welded joint, it is predicted combined with S–N curves that as the stress decreases, the initial SIF range will further decrease, as shown in Fig. 8. When the maximum stress is about 200 MPa and the fatigue life exceeds  $10^8$  cycles, the initial SIF range of the surface defect is equal to  $\Delta K_{th,i}$ . It is reasonable to believe that after this process, fatigue cracks preferentially initiate from the interior. The fatigue life of this order of magnitude is

**Table 1**Predicted fatigue life of crack-initiation and propagation for internal fracture.

Specimen code	Fatigue stress, $\sigma_{ m max}$ (MPa)	Fatigue life, $N_{\rm f}$ (cycles)	Prediction of $N_{\text{FGA} \rightarrow \text{FiE}}$ (cycles)	Prediction of $N_{\rm FGA}$ (cycles)	$N_{\text{FGA}  o \text{FiE}}/N_{\text{f}}$ (%)	$N_{\rm FGA}/N_{\rm f}(\%)$
1	305	2,060,467	220,452	1,840,015	10.7%	89.30%
2	303	4,975,314	247,886	4,727,428	4.98%	95.02%
3	300	6,497,432	235,309	6,262,123	3.62%	96.38%
4	295	6,629,753	274,265	6,355,488	4.14%	95.86%
5	290	8,147,158	321,040	7,826,118	3.94%	96.06%
6	280	19,091,908	330,003	18,751,905	1.72%	98.28%
7	270	47,032,958	383,498	46,649,460	0.82%	99.18%

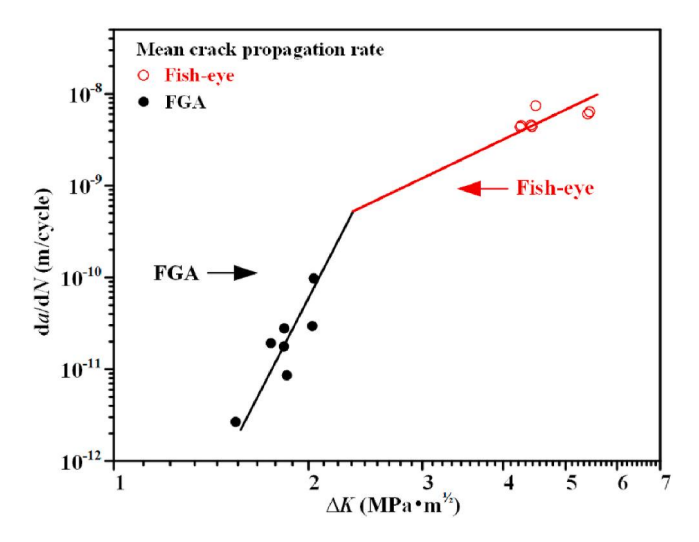


Fig. 10. Evaluation of the mean crack-growth rate in FGA and FiE.

difficult to achieve without using an ultrasonic fatigue machine. One can conclude that the participation of SMRT makes internal fractures appear in advance, the failure mode transition was increased from about 200 MPa to 307 MPa, and the cycles were reduced from  $10^8$  cycles to  $10^6$  cycles, so that the fatigue strengthening of the welded joints is realized under higher stresses and shorter cycles.

#### 5. Conclusions

In the present work, SMRT has been employed on the friction-stirwelded 7075-T651 Al alloy. Uniaxial fatigue tests showed the intervention of the SMRT induced interior-crack initiation under high stress and low cycles (at  $\sim 10^6$  cycles) conditions. Some detailed results can be summarized as follows:

- (1) The fatigue fracture of SMRTed joints presents typical fish-eye characteristics with internal-crack initiation. The formation of FGA is because the crack-extension hindered by the rolled grain boundaries coupled with the action of cyclic loading, the grains at the crack tip are refined, leaving an elliptical extension traces ("beach marks") on the fracture surface. Moreover, the values of the SIF range of the surface and internal modes are calculated. The results show that  $\Delta K_{\text{FGA}}$  keeps constant with an average value of 1.84 MPa $\bullet$ m<sup>1/2</sup>, which is close to the interior-crack-growth threshold ( $\Delta K_{\text{th,i}}$ ), 1.911 MPa $\bullet$ m<sup>1/2</sup> and surface-crack-growth threshold ( $\Delta K_{\text{th,i}}$ ), 1.92 MPa $\bullet$ m<sup>1/2</sup>.
- (2) Based on the Paris-Hertzberg law, it is found that the formation of micro-crack within the FGA consumes most of the fatigue life. When the total fatigue life beyond  $10^7$  cycles, the value of  $N_{\rm FGA}/N_{\rm f}$  is larger than 98%, or over than 99% of  $N_{\rm f}$ . The crack-extension rate within FGA was also estimated. For  $N_{\rm f}$  between  $10^6$  and  $10^7$ , the values of  $({\rm d}a/{\rm d}N)_{\rm FGA}$  are within the range of  $10^{-11}$ – $10^{-12}$  m/cycle. When the fatigue life is higher than  $10^7$  cycles, the order of magnitude of  $({\rm d}a/{\rm d}N)_{\rm FGA}$  enters the order of  $10^{-12}$  m/cycle.
- (3) The enhanced fatigue property accompanied by the suppressed surface-mode fracture in the SMRTed joints might be related to the decreased initial SIF range in the surface layer. According to the change trend of the SIF range of the welded joint, it is predicted when the maximum stress is about 200 MPa, and the fatigue life exceeds 10<sup>8</sup> cycles, fatigue cracks preferentially initiate from the interior. The participation of SMRT makes internal fractures appear in advance, compared with as-welded joints. The stress corresponding to the failure mode transition is increased from about 200 MPa to 307 MPa, and the cycles are reduced from

 $10^8$  cycles to  $10^6$  cycles. Hence, the fatigue strengthening of the welded joints is realized under higher stress and shorter cycle.

#### Data availability

The raw data related to this manuscript will be made available on request.

#### CRediT authorship contribution statement

**Zepeng Liu:** Data curation, Formal analysis, Software, Writing – original draft. **Hongxia Zhang:** Funding acquisition. **Zhenguo Hou:** Visualization, Validation. **Zhifeng Yan:** Investigation. **Peter K. Liaw:** Writing – review & editing. **Peng Dong:** Conceptualization, Supervision, Writing – review & editing.

#### Declaration of competing interest

The authors declare that they have no known competing financial interests or personal relationships that could have appeared to influence the work reported in this paper.

#### Acknowledgements

The present work was supported by National Natural Science Foundation of China (Grant No. 51505321). PKL thanks the support from the National Science Foundation (DMR-1611180 and 1809640) with the program directors, Drs. Judith Yang, Gary Shiflet, and Diana Farkas.

#### References

- T. Naito, H. Ueda, M. Kikuchi, Fatigue behavior of carburized steel with internal oxides and nonmartensitic microstructure near the surface, Metall. Trans. A 15 (1984) 1431–1436. https://link.springer.com/article/10.1007/BF02648572.
- [2] Y. Nakamura, T. Sakai, H. Hirano, K.S. Ravi, Effect of alumite surface treatments on long-life fatigue behavior of a cast aluminum in rotating bending, Int. J. Fatig. 32 (2010) 621–626, https://doi.org/10.1016/j.ijfatigue.2009.10.002.
- [3] Q.Y. Wang, C. Bathias, N. Kawagoishi, Q. Chen, Effect of inclusion on subsurface crack initiation and gigacycle fatigue strength, Int. J. Fatig. 24 (2002) 1269–1274, https://doi.org/10.1016/S0142-1123(02)00037-3.
- [4] Z.G. Yang, S.X. Li, Y.D. Li, Y.B. Liu, W.J. Hui, Q.Y. Wang, Relationship among fatigue life, inclusion size and hydrogen concentration for high-strength steel in the VHCF regime, Mater. Sci. Eng., A 527 (2010) 559–564, https://doi.org/10.1016/j. msea.2009.10.056.
- [5] P. Grad, B. Reuscher, A. Brodyanski, M. Kopnarski, E. Kerscher, Mechanism of fatigue crack initiation and propagation in the very high cycle fatigue regime of high-strength steels, Scripta Mater. 67 (2012) 838–841, https://doi.org/10.1016/j. scriptamat.2012.07.049.
- [6] Y.D. Li, L.L. Zhang, Y.H. Fei, X.Y. Liu, M.X. Li, On the formation mechanisms of fine granular area (FGA) on the fracture surface for high strength steels in the VHCF regime, Int. J. Fatig. 82 (2016) 402–410, https://doi.org/10.1016/j. iifatique. 2015.08.021.
- [7] M.L. Zhu, L. Jin, F.Z. Xuan, Fatigue life and mechanistic modeling of interior microdefect induced cracking in high cycle and very high cycle regimes, Acta Mater. 157 (2018) 259–275, https://doi.org/10.1016/j.actamat.2018.07.036.
- [8] C. Wang, J. Petit, Z.Y. Huang, D. Wagner, Investigation of crack initiation mechanisms responsible for the fish eye formation in the very high cycle fatigue regime, Int. J. Fatig. 119 (2019) 320–329, https://doi.org/10.1016/j. ii/atieue.2018.06.016.
- [9] D. Spriestersbach, E. Kerscher, The role of local plasticity during very high cycle fatigue crack initiation in high-strength steels, Int. J. Fatig. 111 (2018) 93–100, https://doi.org/10.1016/j.jifatigue.2018.02.008.
- [10] C. Bathias, There is no infinite fatigue life in metallic materials, Fatigue Fract. Eng. M. 22 (1999) 559–565, https://doi.org/10.1046/j.1460-2695.1999.00183.x.
- [11] B. Pyttel, D. Schwerdt, C. Berger, Very high cycle fatigue is there a fatigue limit? Int. J. Fatig. 33 (2011) 49–58, https://doi.org/10.1016/j.ijfatigue.2010.05.009.
- [12] J.B. Lai, T. Lund, K. Rydén, A. Gabelli, I. Strandell, The fatigue limit of bearing steels – Part I: a pragmatic approach to predict very high cycle fatigue strength, Int. J. Fatig. 38 (2012) 155–168, https://doi.org/10.1016/j.ijfatigue.2011.09.015.
- [13] Q.Y. Wang, N. Kawagoishi, Q. Chen, Fatigue and fracture behaviour of structural Al-alloys up to very long life regimes, Int. J. Fatig. 28 (2006) 1572–1573, https://doi.org/10.1016/j.ijfatigue.2005.09.017.
- [14] L.P. Xu, Q.Y. Wang, M. Zhou, Micro-crack initiation and propagation in a high strength aluminum alloy during very high cycle fatigue, Mater. Sci. Eng., A 715 (2018) 404–413, https://doi.org/10.1016/j.msea.2018.01.008.

- [15] Y. Chen, C. He, F.L. Liu, C. Wang, Q. Xie, Q.Y. Wang, Y.J. Liu, Effect of microstructure inhomogeneity and crack initiation environment on the very high cycle fatigue behavior of a magnesium alloy, Int. J. Fatig. 131 (2020) 105376, https://doi.org/10.1016/j.jifatigue.2019.105376.
- [16] Z.Q. Lei, Y.S. Hong, J.J. Xie, C.Q. Sun, A.G. Zhao, Effects of inclusion size and location on very-high-cycle fatigue behavior for high strength steels, Int. J. Fatig. 558 (2012) 234–241, https://doi.org/10.1016/j.msea.2012.07.118.
- [17] A.S. Wan, J.J. Xiong, Effect of stress ratio on HCF and VHCF properties at temperatures of 20 °C and 700 °C for nickel-based wrought superalloy GH3617M, Chin. J. Aeronaut. 32 (2019) 2199–2210, https://doi.org/10.1016/j. cia.2019.01.026.
- [18] K. Tokaji, H. Kariya, Mean stress dependence of fatigue strength and subsurface crack initiation in Ti-15Mo-5Zr-3Al alloy, Mater. Sci. Eng., A 281 (2000) 268-274, https://doi.org/10.1016/S0921-5093(99)00710-8.
- [19] C.M. Sonsino, Course of SN-curves especially in the high-cycle fatigue regime with regard to component design and safety, Int. J. Fatig. 29 (2007) 2246–2258, https://doi.org/10.1016/j.ijfatigue.2006.11.015.
- [20] G.A. Qian, C.E. Zhou, Y.S. Hong, A model to predict S–N curves for surface and subsurface crack initiations in different environmental media, Int. J. Fatig. 71 (2015) 35–44, https://doi.org/10.1016/j.ijfatigue.2013.11.013.
- [21] K. Shiozawa, M. Murai, Y. Shimatani, T. Yoshimoto, Transition of fatigue failure mode of Ni–Cr–Mo low-alloy steel in very high cycle regime, Int. J. Fatig. 32 (2010) 541–550, https://doi.org/10.1016/j.ijfatigue.2009.06.011.
- [22] P. Dong, Z.P. Liu, X. Zhai, Z.F. Yan, W.X. Wang, P.K. Liaw, Incredible improvement in fatigue resistance of friction stir welded 7075-T651 aluminum alloy via surface mechanical rolling treatment, Int. J. Fatig. 124 (2019) 15–25, https://doi.org/ 10.1016/j.ijfatigue.2019.02.023.
- [23] T. Sakai, Y. Sato, N. Oguma, Characteristic S-N properties of high-carbon-chromium-bearing steel under axial loading in long-life fatigue, Fatigue Fract. Eng. M. 25 (2002) 765–773, https://doi.org/10.1046/j.1460-2695.2002.00574.x.
- [24] Z. Duan, H. Shi, X. Ma, Fish-eye shape prediction with gigacycle fatigue failure, Fatigue Fract. Eng. M. 34 (2011) 832–837, https://doi.org/10.1111/j.1460-2695.2011.01576.x.
- [25] K. Shiozawa, L. Lu, S. Ishihara, S–N curve characteristics and subsurface crack initiation behaviour in ultra-long life fatigue of a high carbon–chromium bearing steel, Fatigue Fract. Eng. M. 24 (2001) 781–790, https://doi.org/10.1046/j.1460-2695.2001.00459 x.
- [26] K. Shiozawa, Y. Morii, S. Nishino, L. Lu, Subsurface crack initiation and propagation mechanism in high-strength steel in a very high cycle fatigue regime, Int. J. Fatig. 28 (2006) 1521–1532, https://doi.org/10.1016/j. iifatigue.2005.08.015.

- [27] Y. Murakami, T. Nomoto, T. Ueda, Factors influencing the mechanism of superlong fatigue failure in steels, Fatigue Fract. Eng. M. 22 (1999) 581–590, https://doi.org/ 10.1046/j.1460-2695.1999.00187.x.
- [28] Y. Hong, X. Liu, Z. Lei, C. Sun, The formation mechanism of characteristic region at crack initiation for very-high-cycle fatigue of high-strength steels, Int. J. Fatig. 89 (2016) 108–118, https://doi.org/10.1016/j.ijfatigue.2015.11.029.
- [29] Y. Murakami, M. Takada, T. Toriyama, Super-long life tension-compression fatigue properties of quenched and tempered 0.46% carbon steel, Int. J. Fatig. 20 (1998) 661–667, https://doi.org/10.1016/S0142-1123(98)00028-0.
- [30] L. Lu, K. Shiozawa, Y. Morii, Gigacycle fatigue behavior and fracture morphology of high speed tool steel, JIS SKH 51, Trans. Jpn. Soc. Mech. Eng. 69A (2003) 662–670, https://doi.org/10.1299/kikaia.69.662.
- [31] T. Sakai, Review and prospects for current studies on very high cycle fatigue of metallic materials for machine structural use, J. Solid Mech. Mater. Eng. 3 (2009) 425–439, https://doi.org/10.1299/jmmp.3.425.
- [32] T. Sakai, N. Oguma, A. Morikawa, Microscopic and nanoscopic observations of metallurgical structures around inclusions at interior crack initiation site for a bearing steel in very high-cycle fatigue, Fatigue Fract. Eng. M. 38 (2015) 1305–1314, https://doi.org/10.1111/ffe.12344.
- [33] Y.S. Hong, Z.Q. Lei, C.Q. Sun, A.G. Zhao, Propensities of crack interior initiation and early growth for very-high-cycle fatigue of high strength steels, Int. J. Fatig. 58 (2014) 144–151, https://doi.org/10.1016/j.ijfatigue.2013.02.023.
- [34] A.G. Zhao, J.J. Xie, C.Q. Sun, Z.Q. Lei, Y.S. Hong, Prediction of threshold value for FGA formation, Int. J. Fatig. 528 (2011) 6872–6877, https://doi.org/10.1016/j. msea 2011 05 070
- [35] S. Stannzl-Tschegg, B. Schönbauer, Near threshold fatigue crack propagation and internal cracks in steel, Process Eng. 2 (2010) 1547–1555, https://doi.org/ 10.1016/j.proeng.2010.03.167.
- [36] G.A. Qian, Y.S. Hong, C.E. Zhou, Investigation of high cycle and Very-High-Cycle Fatigue behaviors for a structural steel with smooth and notched specimens, Eng. Fail. Anal. 17 (2010) 1517–1525, https://doi.org/10.1016/j. engfailanal.2010.06.002.
- [37] Y. Murakami, S. Kodama, S. Konuma, Quantitative evaluation of effects of nonmetallic inclusions on fatigue strength of high strength steels. I: basic fatigue mechanism and evaluation of correlation between the fatigue fracture stress and the size and location of non-metallic inclusions, Int. J. Fatig. 11 (1989) 291–298, https://doi.org/10.1016/0142-1123(89)90054-6.
- [38] I. Marines-Garcia, P.C. Paris, H. Tada, C. Bathias, Fatigue crack growth from small to long cracks in very-high-cycle fatigue with surface and internal "fish-eye" failures for ferrite-perlitic low carbon steel SAE 8620, Mater. Sci. Eng., A 468–470 (2007) 120–128, https://doi.org/10.1016/j.msea.2006.08.131.